Method for Determining Nozzle Throat Erosion History in Hybrid Rockets

Landon Kamps[1], Yuji Saito[2], Ryosuke Kawabata[3], Masashi Wakita[4], Tsuyoshi Totani[5], Yusuke Takahashi[6]
Hokkaido University, Sapporo, Hokkaido, 060-8628 Japan

and
Harunori Nagata[7]
Hokkaido University, Sapporo, Hokkaido, 060-8628 Japan

The authors of this paper introduce a new reconstruction technique titled Nozzle Throat Reconstruction Technique to estimate nozzle throat erosion history and oxidizer-to-fuel mass ratio history in hybrid rockets. Nine static firing tests were carried out on a 2kN-class Cascaded Multistage Impinging-jet type hybrid rocket motor under varying oxidizer flowrates to evaluate the accuracy of reconstructed results. Nozzle throat erosion histories calculated by the Nozzle Throat Reconstruction Technique agreed well with measured values for initial nozzle throat radius, and successfully reconstructed the case where no measurable amount of nozzle throat erosion occurred. For equivalence ratios 0.6-1.4, the relationship between nozzle throat erosion rate and equivalence ratio of reconstructed results display a trend consistent with chemical kinetic limited heterogeneous combustion theory, as well as predictions made by previous researchers.

Nomenclature

A	=	(nozzle) cross-sectional area
A_r	=	(nozzle) expansion ratio
b	=	measurement precision limit
B	=	measurement bias
C	=	orifice flow coefficient

[1] Master's Course Student, Department of Mechanical and Space Engineering, Member AIAA
[2] Doctor's Course Student, Department of Mechanical and Space Engineering, Student Member AIAA
[3] Master's Course Student, Department of Mechanical and Space Engineering
[4] Assistant Professor, Faculty of Engineering, Laboratory of Space Systems, Member AIAA
[5] Associate Professor, Faculty of Engineering, Laboratory of Space Systems, Member AIAA
[6] Assistant Professor, Faculty of Engineering, Computational Fluid Mechanics Laboratory, Member AIAA
[7] Professor, Faculty of Engineering, Laboratory of Space Systems, Member AIAA.

c^*	=	characteristic exhaust velocity
D	=	(nozzle) diameter
f, g	=	functions representative of NASA CEA operations
F	=	thrust
$\dot{m}$	=	mass flowrate
M	=	(fuel) mass consumption
P	=	pressure
R	=	(nozzle) radius
t	=	(firing) time
x	=	arbitrary parameter
γ	=	(combustion gas) specific heat ratio
η^*	=	characteristic exhaust velocity c^* efficiency
λ	=	thrust correction factor
ξ	=	oxidizer-to-fuel mass ratio, “O/F”
ρ	=	density
σ	=	(nozzle measurement) standard deviation
υ	=	(dynamic measurement) variance
Φ	=	equivalence ratio
$\bar{}$	=	over-bar, to indicate a time-averaged value

Subscripts

a	=	atmosphere
cal	=	calculated value, to distinguish from an experimental value
d	=	(firing) duration
dw	=	orifice downstream position
e	=	nozzle exit plane
f	=	final
fil	=	filtered value, to distinguish from an unfiltered value

i	=	summation counter
o	=	initial
ox	=	oxidizer
st	=	start-up (transient)
sh	=	shut-down (transient)
t	=	nozzle throat plane
up	=	orifice upstream position

I. Introduction

OVER the past 80 years, hybrid rocket motors (HRM) have been the subject of extensive research and development. In an effort to match the performance of traditional solid or liquid bi-propellant rockets, much of this research has been focused on understanding and improving solid fuel regression rate in motors of varying operating conditions and size [1, 2]. As a result, there exists a number of models allowing for the correlation of experimental data for both diffusion limited and chemical kinetic limited heterogeneous combustion between oxidizing gas and solid fuel in hybrid rockets [3]. Throughout the same period of time, research on solid rocket motor (SRM) nozzles has revealed that erosion in the nozzle throat is primarily the result of chemical interactions between the nozzle wall and oxidants in the hot exhaust gas passing over it [4, 5], and that for nonmetallized solid fuel propellants erosion is kinetic limited [6]. The topic of nozzle erosion in hybrid rockets is identified by K. Kuo and M. Chiaverini as an area of concern for future HRM development [2], but there have been no experimental investigations published to date.

The phenomenon known as “O/F shift” stands as a major barrier between the hybrid rocket researcher and experiments for evaluating nozzle erosion. Even in the simplest solid fuel grain designs, hybrid rockets are prone to a shift in oxidizer-to-fuel mass ratio ξ as the burning surface area changes during firing [3, 7]. The non-linear relationship between ξ, burning surface area, and solid fuel regression rate complicates attempts to determine the composition of gas at the nozzle entrance, and limits our ability to understand the mechanism of nozzle erosion through end-point or time-averaged analysis. D. Bianchi and F. Nasuti recently reported results from an extensive numerical investigation into chemical erosion for typical hybrid rocket propellant combinations and revealed that hybrid rocket motors are likely to see 1.5-3 times the nozzle erosion in similar solid rocket motors, due largely in part to the increased presence of oxidizing agents in the combustion product gas [8]. Furthermore, they indicated

that the nozzle erosion rate in hybrid rocket motor propellant combinations is particularly sensitive to ξ, and that maximum erosion rate is expected to take place under slightly oxidizer rich conditions. These findings provide valuable insight into understanding how chemical erosion in HRMs differs to that in SRMs, but have yet to be experimentally verified.

Previous researchers have used reconstruction techniques to estimate the performance of hybrid rockets using experimental data in cases where the nozzle throat erosion was negligibly small. E. J. Wernimont and S.D. Heister demonstrated that regression rate and ξ histories can be reconstructed by solving the characteristic exhaust velocity c^* equation under the condition that overall fuel mass consumption matches observed values [9]. C. Carmicino and A. Sorge considered both the c^* equation and equation of thrust to evaluate time-dependency of nozzle discharge coefficient and c^* efficiency η^* [10]. Most recently, Nagata et al. verified the accuracy of ξ histories reconstructed using the c^* equation by comparing fuel consumption across a series of experiments conducted at the same operating conditions but varying firing durations [11].

Large-scale Cascaded Multistage Impinging-jet (CAMUI) type hybrid rocket development is currently facing the issue of performance loss due to nozzle throat erosion. In FY14, the first series of 15kN-class CAMUI-type HRMs underwent static firing tests and suffered unacceptable levels of nozzle erosion. In one test, the nozzle throat area increased 17% in 15 seconds, which corresponded to a loss in specific impulse of 7 seconds and risk to the structural integrity of the nozzle itself. The method introduced in the following sections, titled "Nozzle Throat Reconstruction Technique" or "NTRT," was developed and tested by the authors with the objective of identifying a reliable measurement technique to carry out future experimental investigations into nozzle erosion in hybrid rockets. NTRT builds from the governing equations and concepts of the reconstruction techniques introduced in Ref. [9-11] to reconstruct the nozzle throat radius R_t and ξ histories through data reduction of commonly measured experimental values: (1) oxidizer mass flowrate, $\dot{m}_{ox}$; (2) (aft) chamber pressure, P_c; (3) thrust, F; (4) overall fuel mass consumed, M_f; and either (5a) final nozzle throat radius, $R_{t,f}$; or (5b) nozzle exit pressure, P_e, in the case that $R_{t,f}$ is not obtainable.

II. Nozzle Throat Reconstruction Technique [NTRT]

In general, reconstruction techniques offer a low-cost and versatile solution to estimating parameters in high enthalpy flows that would otherwise require extravagant and expensive direct measurement techniques. The

underlying concept of NTRT is to estimate regression of the nozzle throat surface by estimating the radius of the fluid column passing through it. This is done by solving the governing equations for compressible flow for converging diverging ducts in conjunction with the governing equations for rocket performance.

Solutions to NTRT are independent of the nozzle material, and thus may be applied to any nozzle shape or material as long as the assumptions behind the governing equations are satisfied. It will be shown in the following sections that the challenge behind successfully employing a reconstruction technique such as NTRT lies in understanding what experimental values may be applied to the simplified flow theory, as well as interpreting the uncertainty associated with said measurements.

A. Governing Equations

The foundation of NTRT is the well-known equation of thrust F:

$$F = \lambda u_e \dot{m} + \left(P_e - P_a\right) A_e \tag{1}$$

where λ, u_e, $\dot{m}$, P_e, P_a, and A_e are thrust correction factor, nozzle exit velocity, propellant mass flowrate, exit pressure, atmospheric pressure and nozzle exit cross-sectional area. This equation serves to connect experimentally measured thrust to one-dimensional ideal nozzle flow theory. In NTRT, calculations begin by solving chemical equilibrium equations for theoretical characteristic exhaust velocity c^* and specific heat ratio γ using NASA CEA [12] for a given P_c and ξ:

$$c^* = f\left(P_c, \xi\right) \tag{2}$$

$$\gamma = g\left(P_c, \xi\right) \tag{3}$$

Propellant mass flowrate $\dot{m}$ is calculated for a given oxidizer mass flowrate $\dot{m}_{ox}$ by:

$$\dot{m} = \dot{m}_{ox}\left(1 + \frac{1}{\xi}\right) \tag{4}$$

Nozzle throat area is calculated explicitly for a given c^* efficiency η^* by:

$$A_t = \frac{\dot{m}\eta^* c^*}{P_c} \tag{5}$$

The value for theoretical exit pressure P_e is determined implicitly from Eq. (6):

$$\left(\frac{P_e}{P_c}\right)^{\frac{1}{\gamma}} \sqrt{\frac{\gamma+1}{\gamma-1}\left[1-\left(\frac{P_e}{P_c}\right)^{\frac{\gamma-1}{\gamma}}\right]} = \frac{A_t}{A_e}\left(\frac{\gamma+1}{2}\right)^{\frac{1}{1-\gamma}} \tag{6}$$

And theoretical exit velocity u_e is calculated explicitly by:

$$u_e = c^* \sqrt{\frac{2\gamma^2}{\gamma-1}\left(\frac{2}{\gamma+1}\right)^{\frac{\gamma+1}{\gamma-1}}\left[1-\left(\frac{P_e}{P_c}\right)^{\frac{\gamma-1}{\gamma}}\right]} \tag{7}$$

Lastly, overall fuel mass consumption M_f is calculated by:

$$M_f = \int \frac{\dot{m}_{ox}}{\xi} dt \tag{8}$$

B. Computational Method

Two computational methods that allow for a solution to the system of equations Eqs. (1)-(8), henceforth referred to as "Method 1" and "Method 2," will be compared in the following sections. Method 1 offers the best results and will be the default method used for computations throughout this study. A detailed flowchart of Method 1 is shown in Fig. 1. In "Method 1," the thrust correction factor λ and characteristic exhaust velocity efficiency η^* are assumed to be constants, allowing for the governing equations to be solved by employing three iterative loops: (Loop A) an outer loop which iterates for η^* based on final nozzle throat radius $R_{t,f}$, (Loop B) an intermediate loop which iterates for λ based on overall fuel mass consumed M_f ; and (Loop C) an inner loop which iterates for ξ based on thrust F at

every time step. A complete history of η^* and λ iterations is shown in Fig. 2, where it can be seen that every η^* iteration (in red) is matched by a complete set of λ iterations (in black). All such iterations in this study were carried out using the bi-section iterative technique, where the initial upper and lower limits for both η^* and λ were zero and two. As is shown in Fig. 2, large changes in the η^* iterations do not greatly affect the new starting point for λ iterations. In Test 1, λ consistently converged to values between 0.884 and 0.902, or roughly within 2% of the nominal value.

Final nozzle throat radius was selected as the convergence criteria for η^* based on the form of Eq. (5). Nozzle throat area A_t is linearly related to η^*, rather any adjustment of η^* directly results in an adjustment of the erosion history. This is evident in Fig. 3, which shows the effect of η^* on the nozzle throat erosion history in Test 1. The values of η^* chosen for this figure were taken from the actual iteration history in Test 1, and are listed in Fig. 2 as "λ Iteration" number 18 ($\eta^* = 1.000$), number 71 ($\eta^* = 0.8750$), and number 217 ($\eta^* = 0.9556$).

Overall fuel mass consumption was selected as the convergence criteria for λ, which is the thrust correction factor in Eq. (1) that enables ξ to be solved for in Loop C. Increasing λ equates to a reduction in energy losses in the flow through the nozzle, and thus an apparent improvement in fuel efficiency. The effect of this relationship is seen in Fig. 4, which shows increased fuel mass consumption rate for smaller values of λ. The values of λ chosen for Fig. 4 are listed in Fig. 2 as "λ Iteration" number 197 ($\lambda = 1.000$), number 199 ($\lambda = 0.8750$), and number 215 ($\lambda = 0.9013$).

In "Method 2," a nozzle exit pressure measurement taken from a static pressure port near the nozzle exit plane is used to solve the governing equations. The additional input data allows for η^* to be solved as a time-dependent variable, and alleviates the need to check results against the final nozzle throat radius $R_{t,f}$. It is in situations where the final nozzle throat radius cannot be measured – when a nozzle breaks apart etc. – that the governing equations are solved using Method 2. In general, Method 2 does not reconstruct a reliable nozzle throat erosion history because the nozzle exit pressure measurement is incompatible with assumptions made in the derivation of the governing equations. This topic is discussed in greater deal in the results section. A simplified flowchart comparing both methods is shown in Fig. 5.

C. Experimental Methodology

All of the measurements required to employ NTRT can be obtained with minimal modification to a conventional HRM set-up. A generalized depiction of the HRM used in this research is shown in Fig. 6. The tests conducted in this study were carried out on a 2kN-class CAMUI-type HRM using high-density polyethylene (HDPE) and liquid

oxygen (LOX) as propellants. Oxidizer was supplied by using high pressure helium as a pressurant, and the flowrate was determined by measuring the pressure drop across an orifice plate $\Delta P_{up,dw}$ according to Eq. (9):

$$\dot{m}_{ox} = C\sqrt{2\rho\Delta P_{up,dw}} \tag{9}$$

where C is an experimentally determined orifice flow coefficient, and ρ is the LOX density. The temperature of LOX T_{up} was measured upstream of the orifice plate and used to estimate the quality of a two-phase oxidizer supply during start-up. It is important to point out that any device capable of measuring flowrate can be used when employing NTRT. Also, nozzle exit pressure was measured from a static pressure port located along the nozzle wall near the nozzle exit plane to evaluate the applicability of such a measurement for NTRT, but this value is not necessary for default NTRT computations using Method 1. The minimum required experimental data necessary to carry out NTRT are:

1) Oxidizer mass flowrate, $\dot{m}_{ox}$
2) Thrust, F
3) (aft) Chamber pressure, P_c
4) Overall fuel mass consumption, M_f
5) Final nozzle throat radius, $R_{t,f}$

This data for Test 1 is shown in Fig. 7, which shows each value plus/minus the measurement uncertainty.

D. Data Acquisition and Processing

As required for NTRT, multiple dynamic and static measurements were taken during the experiments conducted in this study. Pressure and thrust were recorded at 200 [Hz] using KYOWA DCS-100A series software. All pressure measurements were taken with KYOWA PHB-A-10MPa pressure sensors rated to plus/minus 0.0404 [MPa], with the exception of nozzle exit pressure measurements in Tests 4-6 which were taken with a KYOWA PHB-A-2MPa sensor rated to plus/minus 0.0028 [MPa] in accuracy. Thrust was measured with a KYOWA LMB-A-2kN load cell rated to plus/minus 14.1 [N]. These instruments were calibrated by the manufacturer, such that rated accuracies

account for uncertainty due to nonlinearity, hysteresis, low-temperature conditions and external loading. As a precautionary measure, all sensors were tested simultaneously against the same pressure source before each experiment to ensure that there were no abnormalities. During post processing, pressure and thrust measurements were filtered using a 20-point moving average. The reason for applying a moving average was to reduce the presence of oscillations in reconstructed nozzle throat erosion histories, which ultimately lead to undiscernible linear approximations for nozzle throat erosion rate. The uncertainty introduced by applying a moving filter is described in the uncertainty analysis section of this paper (Section II E.). Initial and final nozzle throat diameter measurements were taken with a MonotaRO digital caliper rated to plus/minus 0.01 [mm]. Initial and final fuel mass was measured using an A&D EK-4100i digital scale rated to plus/minus 0.1 [g].

Nozzle throat diameter measurements were repeated twelve times before and after each experiment. The set of measurements taken for Test 1 is shown in Table 1. The diameter is measured at 0°, 45°, 90° and 135° in reference to the chamber pressure port inlet, and this set of measurements is repeated three times. The standard deviation of these measurements σ_D and precision limit of the digital caliper b_D are used to determine the measurement uncertainty U_D according to Eq (10).

$$U_D{}^2 = (2\sigma_D)^2 + b_D{}^2 \tag{10}$$

In this way, non-circular erosion can be accounted for through an increase in σ_D.

A detailed schematic of the nozzle assembly used in Tests 1-3 is shown in Fig.8. It is important to note that the governing Eqs. (6) and (7) are based on the assumption that the velocity of gas in the chamber is negligibly small compared with that of gas entering the nozzle. For this reason, a pressure port was placed away from the nozzle throat entrance. Furthermore, Eqs. (6) and (7) are based on the assumption that there is no radial pressure distribution in the diverging section of the nozzle, which limits our ability to use exit pressure measurements taken from the exit pressure port as shown in in Fig. 8

The procedure for identifying the firing duration was adapted from Ref. [13, p. 459]. In this reference, there is a distinction between two times, “burn time” and “action time,” which encompass the transients observed during start-up and shut-down in static firing tests. The definition for burn time is used for determining “firing duration” or t_d in this report. The initial time t_o is defined as the time when the chamber (gauge) pressure reaches ten percent of its

maximum value. The final time t_f is defined by the time where the chamber (gauge) pressure history intersects the aft-tangent bisector. The selection of these times in Test 1 is depicted in Fig. 9. The start-up transient t_{st} is identified by the interval between 10-75% maximum chamber pressure, and the shut-down transient t_{sh} is defined by the interval between the aft-tangent bisector intersection and the final 10% maximum chamber pressure time. These transients are used in uncertainty analysis as precision limits for the designation of firing duration.

E. Uncertainty Analysis

Uncertainty in reconstructed solutions is determined by analyzing the bias introduced from experimental measurements. The overall uncertainty U_y in some NTRT output y is calculated from Eq. (11):

$$\begin{aligned} U_y{}^2 &= \sum\left(\frac{\partial y}{\partial x_i}U_{x_i}\right)^2 \\ &= \left(\frac{\partial y}{\partial \dot{m}_{ox}}U_{\dot{m}_{ox}}\right)^2 + \left(\frac{\partial y}{\partial P_c}U_{P_c}\right)^2 + \left(\frac{\partial y}{\partial F}U_F\right)^2 + \left(\frac{\partial y}{\partial M_f}U_{M_f}\right)^2 + \left(\frac{\partial y}{\partial R_{t,f}}U_{R_{t,f}}\right)^2 + \left(\frac{\partial y}{\partial t_o}U_{t_o}\right)^2 + \left(\frac{\partial y}{\partial t_f}U_{t_f}\right)^2 \end{aligned} \tag{11}$$

where x_i represents an experimental measurement and the U-terms on the right hand side represent the uncertainty in that measurement. The uncertainties in pressure and thrust measurements are determined by Eq. (12):

$$U^2 = b^2 + \upsilon^2 \tag{12}$$

Where b represents the precision limit of the pressure sensor or load cell, and υ is a measure of variance between the filtered and unfiltered data calculated by Eq. (13):

$$\upsilon^2 = \frac{1}{N}\sum_{i=1}^{N}(x_i - x_{fil,i})^2 \tag{13}$$

Here, x_i represents the unfiltered pressure or thrust data, and $x_{fil,i}$ represents the value of filtered data at the corresponding time. Thus, the uncertainty in oxidizer mass flowrate can be calculated according to Eq. (14):

$$U_{\dot{m}_{ox}}{}^{2} = \left(\frac{\partial y}{\partial P_{up}} U_{P_{up}}\right)^{2} + \left(\frac{\partial y}{\partial P_{dw}} U_{P_{dw}}\right)^{2} = \left(\frac{\partial y}{\partial P_{up}} \sqrt{b_{P_{up}}{}^{2} + \upsilon_{P_{up}}{}^{2}}\right)^{2} + \left(\frac{\partial y}{\partial P_{dw}} \sqrt{b_{P_{dw}}{}^{2} + \upsilon_{P_{dw}}{}^{2}}\right)^{2} \tag{14}$$

The uncertainty in fuel mass consumption is simply the precision limit of the digital scale because there was no scatter in the data between repeated measurements. The uncertainties in designating the initial and final times are one-half of the start-up and shut-down transients, respectively.

The partial derivative terms in Eq. (11) represent the sensitivity of the reconstructed solution to each input. Since Eqs. (1)-(8) are a coupled nonlinear system of equations, these sensitivities are approximated by the linearized Eq. (15):

$$\frac{\partial y}{\partial x_i} \cong \frac{y(t, x_i + \Delta x_i) - y(t, x_i)}{\Delta x_i} \tag{15}$$

Here, the numerator is the change in NTRT solution y given that the input parameter x_i has been perturbed by the amount Δx_i. In this study, Δx_i was selected to be 1% of the nominal experimental value. This perturbation-type sensitivity analysis is similar to that introduced by R. A. Frederick and B. E. Greiner for determining uncertainty of various parameters in laboratory scale HRM performance analysis [14].

Erosion rates are estimated by a linear approximation of the derivative of nozzle throat erosion history data according to Eq. (16):

$$\frac{\partial R_t}{\partial t} \cong \frac{R_t(t + \Delta t) - R_t(t)}{\Delta t} \tag{16}$$

In this case, confidence bounds for erosion rate are taken as the local overall erosion measurement bias distributed across the entire firing time. The reason for the distribution of uncertainty across the entire firing time is based on the idea that erosion history should lay within the confidence bounds, erosion history should be steady and continuous in absence of mechanical/structural failure, and erosion rate must be greater than or equal to zero. These conditions essentially state that confidence bounds for erosion rate must be determined in consideration of the entire erosion history, and not solely on a point-by-point basis.

III. Results

In total, nine firing tests were conducted using a 2kN-class CAMUI-type HRM to investigate the results obtained by NTRT under varying experimental conditions and nozzle materials. Tests 1-3 employed a graphite nozzle with expansion ratio A_r = 4.9 [-]. Tests 4-6 employed a graphite nozzle with expansion ratio A_r = 2.3 [-]. Tests 7 and 8 employed a Silicon Carbide (SiC) coated graphite nozzle throat insert and Carbon Fiber Reinforced Ceramic (CFRC) nozzle throat insert, respectively – both with expansion ratio A_r = 4.9 [-]. Test 9 employed a SiC nozzle throat insert with expansion ratio A_r = 4.9 [-], which failed structurally during post-combustion purge by gaseous nitrogen. Key experimental data and the results of NTRT for each test are listed in Tables 2 and 3, respectively. It is worth noting that thrust correction factor λ is roughly equal to 0.9 for all tests with the exception of Test 2 and Test 8. Furthermore, the values of combustion efficiency η^* in these two tests are also relatively smaller than that of the other tests. One possible explanation for this result in Test 2 is a severe overexpansion of the exhaust gas leaving the nozzle. In this test, the exhaust plume was significantly less luminescent than in the other tests, with a clear separation of the plume from the nozzle exit wall. This finding is supported by the very low value for nozzle exit pressure listed in Table 2. One possible explanation for the result in Test 8 is the violent nature in which the CFRC nozzle was eroded during firing. In a review of a video recording capturing the exhaust plume in this test, a cloud consisting of pebble-sized pieces of nozzle throat insert could be seen being ejected from the nozzle during the firing. This unusual disturbance in the nozzle flow field is likely the reason the results of NTRT show relatively low efficiencies.

A. NTRT Solutions for Nozzle Throat Erosion History

The solutions for nozzle throat erosion history determined by NTRT for Tests 1-3 and Tests 4-6 are plotted in Fig. 10 and Fig. 11, respectively. With the exception of the transient period during start-up, results of NTRT for Tests 1-6 agree closely with measured values for initial throat radius, and display physically consistent – i.e. continuous and increasing – values for nozzle throat erosion history. The large fluctuations during the first 0.5 seconds in both Fig. 10 and Fig.11 are caused by the presence of two-phase flow in the oxidizer supply line. At the beginning of each test, the oxidizer supply system is at local atmospheric temperature, which is always warm enough to gasify some portion of the LOX and induce a two-phase flow. Typically the LOX supply line is cooled enough in the first 0.5 seconds of testing to prevent any further gasification of LOX before injection into the motor.

In other words, Eq. (9) does not accurately determine flowrate of oxidizer supplied during the first 0.5 seconds of operation. This discrepancy in oxidizer flowrate calculation leads to an unrealistic erosion history during this time.

The sharp spikes present around 0.5-1.5 seconds in Fig. 10, and not present in Fig. 11, were caused by similar spikes in thrust measurement history. It was found that the thrust sensor grounding wire was only loosely connected to the corresponding grounding rod during these experiments. This connection was adjusted after completing Test 3, and no such oscillations appeared in any of the remaining tests (Tests 4-9). Since these fluctuations were limited to the initial period of firing, the remaining portion of nozzle throat erosion histories are considered in the following analysis. The solutions for nozzle throat erosion history calculated from NTRT for Tests 7 and 8 are plotted in Fig. 12.

The results for Test 7 are especially important to this study because they verify that the nozzle throat erosion history determined using NTRT is remarkably accurate. There was no observable erosion in Test 7, and so the exact solution to the nozzle throat erosion history is simply the initial throat radius. It is evident from Fig. 12 that the solution to NTRT remains extremely close (< 0.2 mm) to the exact value for the majority of the firing duration. Although the material used in Test 8 will not be a candidate for future flight models due to an extremely high erosion rate, the close fit of the NTRT solution to measured values supports the claim that the results do not depend on the nozzle material.

The nozzle throat insert in Test 9 was made of SiC, which cracked during post-combustion motor purging and came apart during disassembly – before a final throat measurement could be made. The large fluctuations during motor start-up due to two-phase flow in the supply line make it difficult to automate the iterative Loop A (see Fig. 1) based on initial nozzle throat radius. Therefore, the authors decided to use the average value for η^* calculated using Method 2 as the input value for NTRT (Method 1) computation, eliminating the need for a final nozzle throat radius $R_{t,f}$ measurement. This judgement was based on two observations: the first being that the η^* history calculated by Method 2 was nearly constant during firing; the second being that C. Carmicino and A. Sorge showed in their study that variations in η^* determined by reconstruction were less than 4% of the time-averaged values and remained nearly constant for the duration of firing [10]. Figures 13 and 14 show the η^* history for Test 9 calculated using Method 2, and a comparison of solutions for nozzle throat erosion history computed from Method 1 and Method 2, respectively.

B. Uncertainty in NTRT Solutions

The breakdown of uncertainty analysis components for Test 1 is listed in Table 4. By examining the sensitivities of key NTRT solutions to their input parameters we can gain insight into how to improve the accuracy of NTRT, as well as what role the constants λ and η^* play in connecting the governing equations to experimental measurements. The uncertainty in nozzle throat erosion history is predominantly governed by the value of the final nozzle throat radius measurement uncertainty, because Loop A of Method 1 always forces the final nozzle throat radius to converge on the experimentally determined value. It is for this reason that a large part of the uncertainty in η^* is the uncertainty in the final nozzle throat radius measurement. For example, a 1% increase/decrease in chamber pressure will cause an similar increase/decrease in nozzle throat erosion history, but Loop A enables such changes in erosion history to be transferred to changes in η^*. This ultimately reduces the uncertainty in nozzle throat erosion history at the expense of increased uncertainty in η^*. Based on results in Table 4, it is also clear that the only way to significantly improve the accuracy of the solution for ξ is to reduce the uncertainty in oxidizer flowrate measurement. Whereas a longer firing duration and more accurate load cell are the best measures to take towards reducing uncertainty in λ.

C. Nozzle Throat Erosion Rate

Experimental measurements of thrust and pressure were recorded at 200 [Hz], and exhibit small scale oscillations between neighboring data points. Linear approximations for erosion based on Eq. (16) were made at a time step of Δt = 0.25 [s] (a span of 50 data points) to ensure values for erosion rate remained positive. Figure 15 plots the nozzle erosion rates of Tests 1-6 as a function of equivalence ratio. D. Bianchi and F. Nasuti showed a similar plot in Ref. [8] based on the results of numerical analysis for an HRM operating at 10 bar with an HTPB/oxygen propellant combination for values of equivalence ratio between $0.5 < \Phi < 2$ [-]. There is a strong similarity between D. Bianchi and F. Nasuti's numerical analysis and the results shown in Fig. 15 for the same range of equivalence ratios. The most remarkable similarity being a local maximum of nozzle throat erosion rate at an equivalence ratio of $\Phi \approx 0.8$ [-]. This agreement shows that the ξ history determined by NTRT is realistic. Furthermore, the erosion rates in Test 4 are roughly twice the value of erosion rates in Test 1 at similar values of equivalence ratio. This is true to a greater extent when comparing Test 5 to Test 2. Considering that the chamber pressure in Test 4 was on average over 30% larger than the chamber pressure in Test 1, and the chamber pressure in Test 5 was over 50% larger than that in Test 2, we can conclude that a pressure dependency of nozzle throat erosion

rate may be apparent in these results. This conclusion is consistent with expectations for chemical kinetic limited heterogeneous combustion, and serves as additional support to the claim that the results of NTRT are realistic.

It is important to point out that nozzle throat erosion rate at values of equivalence ratio $\Phi < 0.5$ [-] do not follow the same trend as those for $\Phi > 0.5$ [-]. The authors' initial expectations for erosion in these experiments was largely based on findings from the numerical analysis reported by D. Bianchi and F. Nasuti. They predicted a sharply decreasing erosion rate in conditions $\Phi < 0.8$ [-], but did not extend their simulation to the regime $\Phi < 0.5$ [-]. The discovery of unexpectedly high erosion rate in highly oxidizer rich conditions highlights the benefits of conducting experiments. Future experiments employing NTRT may be conducted to clarify the difference between erosion in these two regimes.

D. Method 1 and Method 2 Comparison

The authors had two major concerns with using a nozzle exit pressure measurement and Method 2 to close the governing system of equations Eqs. (1)-(8) when designing the experimental apparatus for this study. The first being that the equations for adiabatic expansion, Eqs. (6) and (7) are based on a 1-D approximation of pressure field; in reality, there is a radial pressure distribution at any cross-section, and a static pressure measurement taken from the nozzle wall will deviate from this value. The second being that the gauge pressure of exhaust gas leaving the nozzle is relatively small, requiring a very sensitive pressure sensor for accurate measurements; increasing the cost and/or decreasing the accuracy of measurements.

Two countermeasures were taken between Tests 1-3 and Tests 4-6 to overcome concerns related to gauge pressure. One countermeasure was to decrease the nozzle expansion ratio from $A_r = 4.9$ [-] to $A_r = 2.3$ [-] to lower the pressure drop between the throat and exit planes. The second measure was to employ a high-accuracy pressure sensor; improving the precision limit from $b_{Pe} = 0.0404$ [MPa] to $b_{Pe} = 0.00280$ [MPa]. Figures 16 and 17 compare the results of Method 1 and Method 2 for nozzle throat erosion history in Tests 1 and 4, respectively. There is a noticeably large improvement in the results of Method 2 between Tests 1 and 4. These improvements are supported by the highly improved accuracy of nozzle exit pressure measurements between Tests 1-3 and Tests 4-6 as listed in Table 2.

IV. Discussion

The results of Tests 1-9 attest to the versatility of using NTRT to evaluate nozzle throat erosion history in hybrid rockets with nozzles of various materials, and operating under various flow conditions. The accuracy of results determined by NTRT is validated by grounding computations in physical measurements wherever appropriate, and matching results to predictions or observations made in previous studies. The collection of evidence supporting the validity of results presented in this paper is as follows. First, NTRT is confirmed to reconstruct the nozzle throat erosion history with an error of less than 0.2 [mm] or 2% of the initial throat radius in Test 7 where the exact solution is known. Second, there is close agreement between nozzle throat erosion histories calculated by NTRT and measured values for initial nozzle throat radius in all Tests 1-9. Third, there is a strong similarity in trends between results shown in Fig. 15 and a similar figure from a numerical simulation by D. Bianchi and F. Nasuti in Ref. [8]. In particular, the equivalence ratio which corresponds to a local maximum for nozzle throat erosion rate is roughly the same. Fourth, uncertainty analysis revealed that the appropriate nozzle throat diameter measurement procedure, and selection of accurate sensors can reduce the bias in NTRT solutions to less than 10% of the overall erosion. Fifth, the condition for convergence of Loop B in Method 1 is an agreement of calculated fuel mass consumption to measured values taken before and after firing. Even though there is a lot of support that the results of NTRT presented in this paper are accurate, the authors plan to conduct one additional verification study in the future to confirm the accuracy of ξ directly. This is possible by repeating Test 7 (no erosion case) at different firing times in a fashion similar to Ref. 11.

The contribution of conceptual bias, such as that introduced by firing time designation and the application of data filters, was shown to introduce an acceptably small degree of uncertainty to NTRT solutions. Improving the final nozzle throat diameter measurement and chamber pressure sensor precision are the most cost effective and immediate means of improving accuracy of NTRT for future HRM nozzle erosion research, followed by improving the accuracy of the orifice downstream pressure and orifice upstream pressure measurements.

V. Conclusion

Nozzle erosion in hybrid rockets has yet to be experimentally investigated even though it is an important consideration in large-scale hybrid rocket development. The authors were recently confronted with an unacceptable level of nozzle erosion in 15kN-class CAMUI-type hybrid rocket static firing tests and developed the Nozzle Throat

Reconstruction Technique introduced in this paper. This technique is used for determining nozzle throat erosion history and oxidizer-to-fuel mass ratio in hybrid rockets based on readily available experimental data. Results of the Nozzle Throat Reconstruction Technique are shown to agree well with initial nozzle throat radius in numerous experiments of varying pressure and oxidizer flowrate while exhibiting acceptable experimental uncertainty. Moreover, NTRT was able to very accurately reconstruct the case where no measurable amount of nozzle throat erosion occurred. In situations where final nozzle throat radius cannot be measured, an exit pressure measurement taken from the wall near the nozzle exit may be used instead. This modification will preserve the nozzle erosion trend, but is subject to an overall under/over estimation of erosion due to departure of experimental measurement from one-dimensional flow assumptions in the governing equations.

Acknowledgments

The authors would like to thank Tsutomu Uematsu and the staff at Uematsu Electric Co., Ltd. for their hard work and support in carrying out the static firing tests conducted for this study. This research is supported by the Ministry of Education, Science, Sports and Culture, Grant-in-Aid for Science Research (B). 15H04197, 2016.

References

[1] Altman, D., Holzman, A., "Overview and History of Hybrid Rocket Propulsion," *Fundamentals of Hybrid Rocket Propulsion*, edited by Chiaverini, M. and Kuo, K., Vol. 218, Progress in Astronautics and Aeronautics, AIAA, Washington, DC, 2006, pp. 1-36.

[2] Kuo, K., Chiaverini, M., "Challenges of Hybrid Rocket Propulsion in the 21st Century," *Fundamentals of Hybrid Rocket Propulsion*, edited by Chiaverini, M. and Kuo, K., Vol. 218, Progress in Astronautics and Aeronautics, AIAA, Washington, DC, 2006, pp. 593-638.

[3] Chiaverini, M., "Review of Solid-Fuel Regression," *Fundamentals of Hybrid Rocket Propulsion*, edited by Chiaverini, M. and Kuo, K., Vol. 218, Progress in Astronautics and Aeronautics, AIAA, Washington, DC, 2006, pp. 37-126.

[4] McDonald, A., Hedman, P., "Erosion of Graphite in Solid-Propellant Combust Gases and Effects on Heat Transfer," *AIAA Journal*, Vol. 3, No. 7, 1965, pp. 1250-1257.
doi: 10.2514/3.3117

[5] Acharya, R., Kuo, K., "Effect of Pressure and Propellant Composition on Graphite Rocket Nozzle Erosion Rate," *Journal of Propulsion and Power*, Vol. 23, No. 6, 2007, pp. 1242-1254.
doi: 10.2514/1.24011

[6] Bianchi, D., Nasuti, F., Onofri, M., "Thermochemical Erosion Analysis for Graphite/Carbon-Carbon Rocket Nozzles," *Journal of Propulsion and Power*, Vol. 27, No. 1, 2011, pp. 197-205.
doi: 10.2514/147754

[7] Karabeyoglu, A., Toson, E., Evans, B., "'O/F Shift' in Hybrid Rockets," AIAA Paper 2014-3851, 2014.

[8] Bianchi, D., Nasuti, F., "Numerical Analysis of Nozzle Material Thermochemical Erosion in Hybrid Rocket Engines," *Journal of Propulsion and Power*, Vol. 29, No. 3, 2013, pp. 547-558.
doi: 10.2514/1.834813

[9] Wernimont, E. J., Heister, S. D., "Reconstruction Technique for Reducing Hybrid-Rocket Combustion Test Data," *Journal of Propulsion and Power*, Vol. 15, No. 1, 1999, pp. 128-136.
doi: 10.2514/2.5401

[10] Carmicino, C., Sorge, A. R., "Influence of a Conical Axial Injector on Hybrid Rocket Performance," *Journal of Propulsion and Power*, Vol. 22, No. 5, 2006, pp. 984-995.
doi: 10.2514/1.19528

[11] Nagata, H., Nakayama, H., Watanabe, M., Wakita, M., Totani, T., "Accuracy and Applicable Range of a Reconstruction Technique for Hybrid Rockets," *Advances in Aircraft and Spacecraft Science*, Vol. 1, No. 3, 2014, pp. 273-289.
doi: 10.12989/aas.2014.1.3.273

[12] Gordon, S., McBride, B., "Computer Program for Calculation of Complex Chemical Equilibrium Compositions and Applications," NASA RP-1311, 1994.

[13] Sutton, G., Biblarz, O., "Solid Propellant Rocket Fundamentals," *Rocket Propulsion Elements*, 8th ed., Wiley, New Jersey, 2010, pp.435-489.

[14] Frederick, R. A. Jr., Greiner, B. E., "Laboratory-Scale Hybrid Rocket Motor Uncertainty Analysis," *Journal of Propulsion and Power*, Vol. 12, No. 3, 1996, pp. 605-611.

doi: 10.2514/3.24076

Table 1 - Final Nozzle Throat Diameter $D_{t,f}$ Measurements in Test 1 [mm]

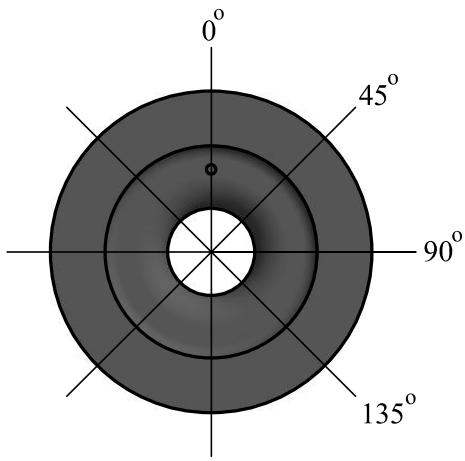

Trial	0°	45°	90°	135°
1	28.46	28.46	28.47	28.37
2	28.46	28.45	28.47	28.38
3	28.47	28.47	28.48	28.37
$\sigma_{D_{t,f}}$	$b_{D_{t,f}}$	$U_{D_{t,f}}$	$\overline{D_{t,f}} \pm U_{D_{t,f}}$	
0.04	0.01	0.08	28.44 ± 0.08	

Table 2 - Summary of Experimental Data

Test [#]	Material [name]	$R_{t,o}$ [mm]	A_r [-]	t_d [s]	$\overline{F}$ [N]	$\overline{P_c}$ [MPa]	$\overline{\dot{m}_{ox}}$ [g/s]	M_f [g]	ΔR_t [mm]	$\overline{P_e}$ [MPa]
1	graphite	13.5	4.9	5.0	1520±2%	1.94±2%	568±2%	785±<1%	0.72±6%	0.10±42%
2	graphite	13.5	4.9	4.9	923±6%	1.33±3%	631±1%	314±<1%	0.64±2%	0.05±85%
3	graphite	13.5	4.9	4.9	1181±14%	1.61±3%	581±1%	499±<1%	0.42±10%	0.08±50%
4	graphite	11.5	2.3	5.0	1479±2%	2.59±2%	497±2%	825±<1%	1.16±9%	0.34±<1%
5	graphite	11.5	2.3	5.0	1223±1%	2.02±2%	625±2%	362±<1%	1.67±17%	0.28±1%
6	graphite	11.5	2.3	9.7	703±15%	1.28±4%	320±6%	478±<1%	0.52±6%	0.16±2%
7	SiC coat	13.5	4.9	5.0	1457±1%	1.95±2%	521±2%	771±<1%	0.00±0.01	0.09±3%
8	CFRC	13.5	4.9	4.9	1242±1%	1.21±3%	547±1%	733±<1%	6.80±11%	0.11±3%
9	SiC	13.5	4.9	5.0	1464±1%	1.94±2%	534±1%	835±<1%	-	0.09±3%

note: plus/minus % terms represent uncertainty

Table 3 - NTRT Results

Test [#]	λ [-]	η^* [-]	$\overline{\xi}$ [-]	$\overline{\dot{R}_t}$ [mm/s]
1	0.901±2%	0.956±2%	5.26±2%	0.17±11%
2	0.784±2%	0.851±3%	11.53±6%	0.16±3%
3	0.886±5%	0.952±5%	9.05±2%	0.11±18%
4	0.946±4%	1.028±4%	3.83±2%	0.32±17%
5	0.910±3%	0.982±3%	9.27±2%	0.45±24%

6	0.906±2%	0.985±3%	7.62±9%	0.11±6%
7	0.912±1%	0.972±2%	3.85±2%	0.06±7%
8	0.829±2%	0.933±3%	4.07±2%	1.65±16%
9	0.898±3%	0.996**	3.78±2%	-

** η^* in Test 9 was input data determined by Method 2

Table 4 - Breakdown of Uncertainty in NTRT Results from Test 1

∂x_i	$\left\lvert \overline{\frac{\partial \lambda}{\partial x_i} U_{x_i}} \right\rvert$	$\left\lvert \overline{\frac{\partial \eta^*}{\partial x_i} U_{x_i}} \right\rvert$	$\left\lvert \overline{\frac{\partial \xi}{\partial x_i} U_{x_i}} \right\rvert$	$\left\lvert \overline{\frac{\partial R_t}{\partial x_i} U_{x_i}} \right\rvert$
	[-]	[-]	[-]	[mm]
1% $\dot{m}_{ox}$	0.006	0.006	0.11	<0.01
1% M_f	0.003	0.003	<0.01	<0.01
1% P_c	0.001	0.010	<0.01	<0.01
1% $R_{t,f}$	<0.001	0.019	<0.01	0.04
1% F	0.009	<0.001	<0.01	<0.01
1% t_o	<0.001	<0.001	-	-
1% t_f	0.012	<0.001	-	-

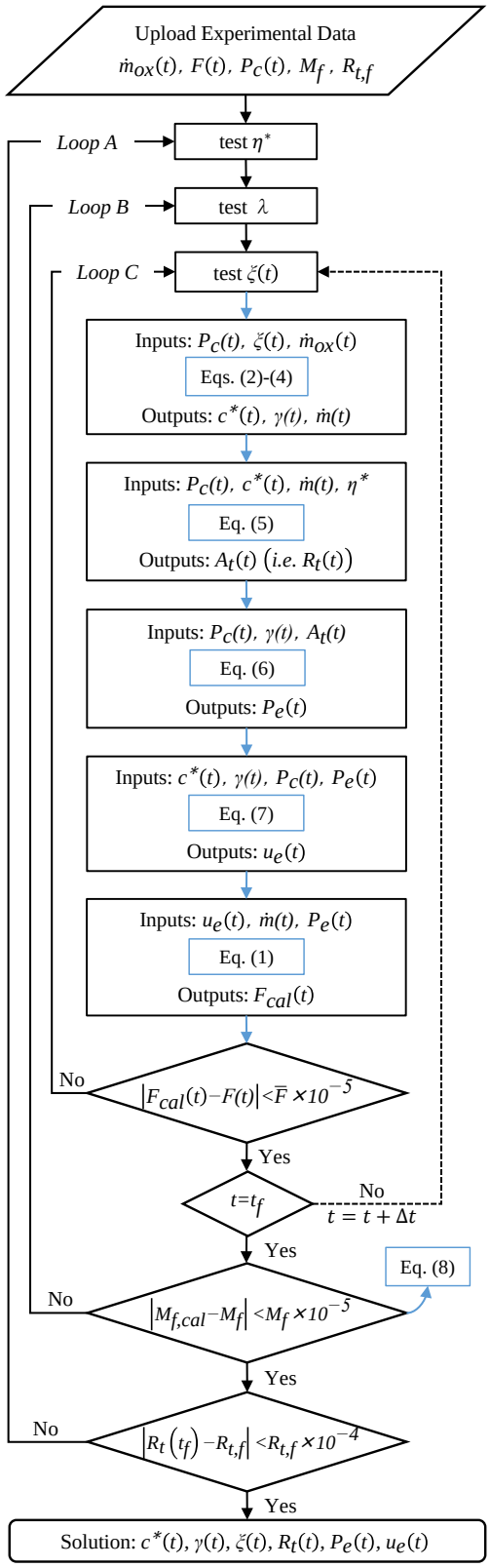

Figure 1. Method 1 flowchart.

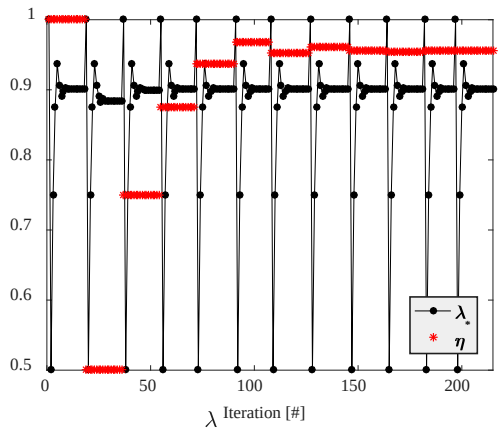

Figure 2. Iteration history of λ and η^* in Test 1.

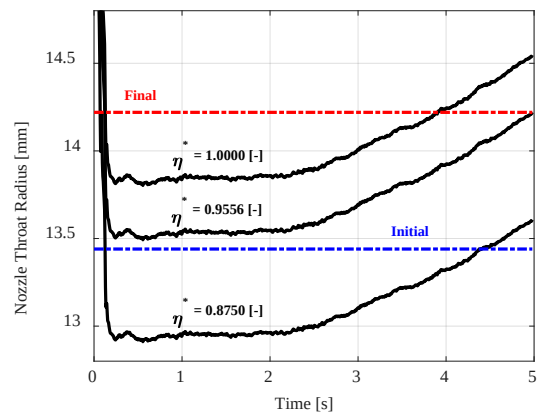

Figure 3. Effect of η^* iteration on nozzle throat erosion history in Test 1.

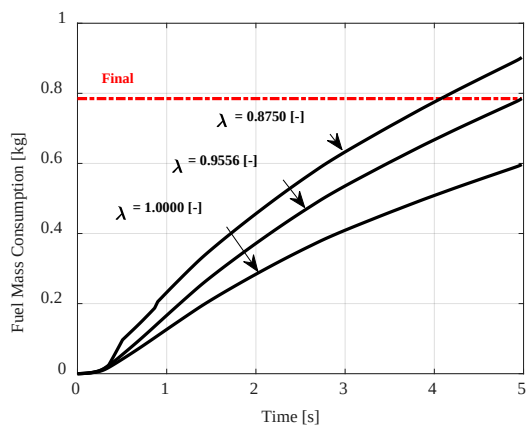

Figure 4. Effect of λ iteration on fuel mass consumption history in Test 1.

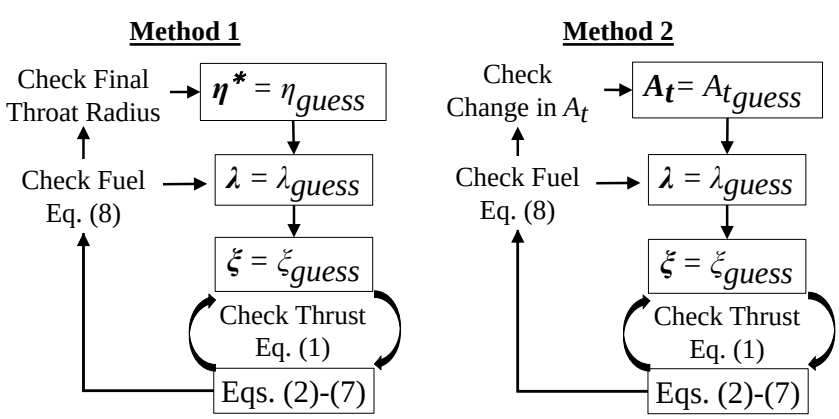

Figure 5. Simplified comparison flowchart of Method 1 and Method 2.

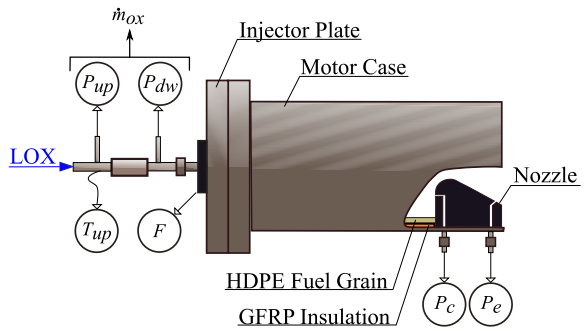

Figure 6. Schematic of HRM and sensor positions.

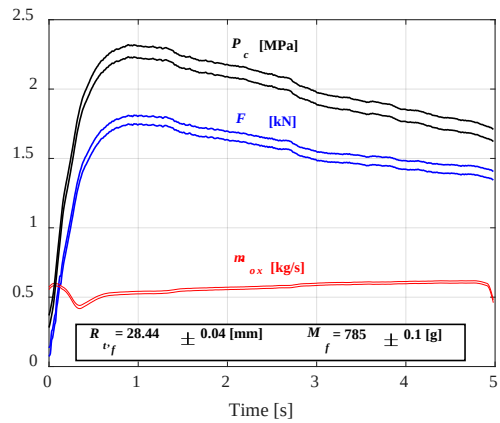

Figure 7. Experimental inputs for NTRT in Test 1 (plus/minus measurement uncertainty).

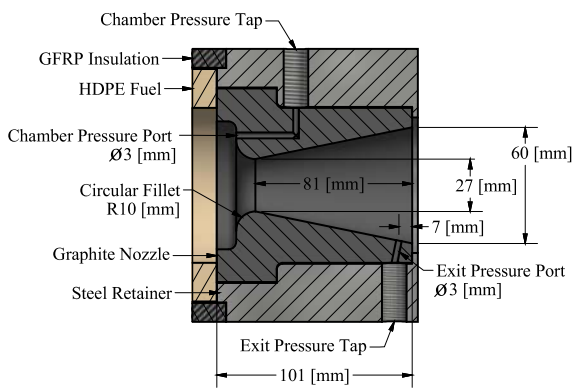

Figure 8. Detailed schematic of nozzle assembly.

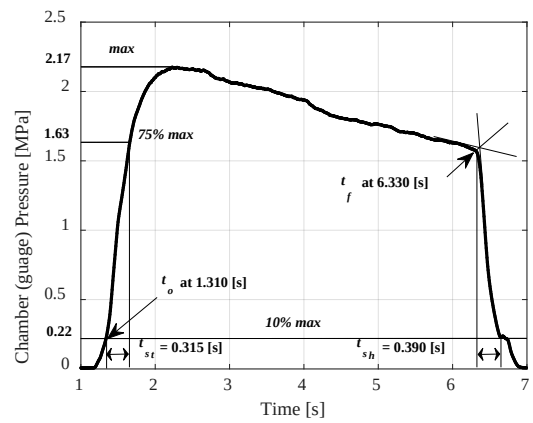

Figure 9. Identifying firing duration, as well as start-up and shut-down transients.

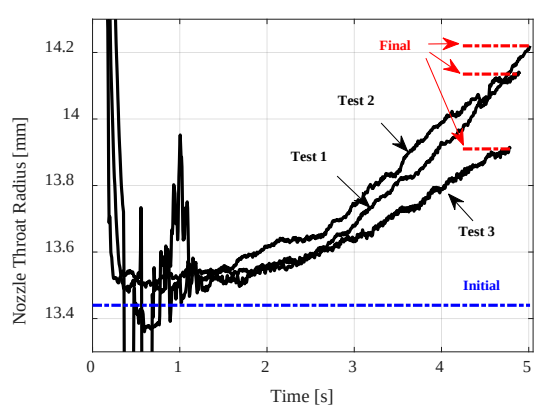

Figure 10. NTRT solutions for nozzle throat erosion history in Tests 1-3. *graphite nozzles; A_r =*

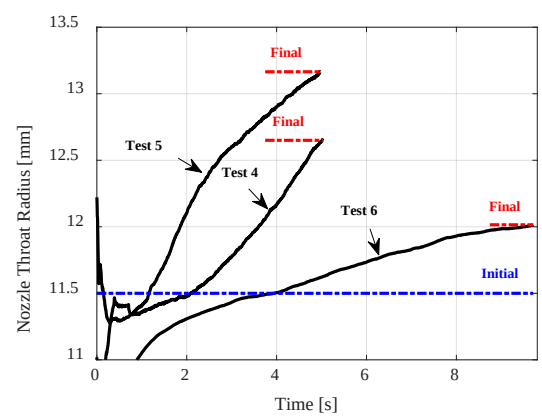

Figure 11. NTRT solutions for nozzle throat erosion history in Tests 4-6. *graphite nozzles; A_r =*

4.9 [-] 2.3 [-]

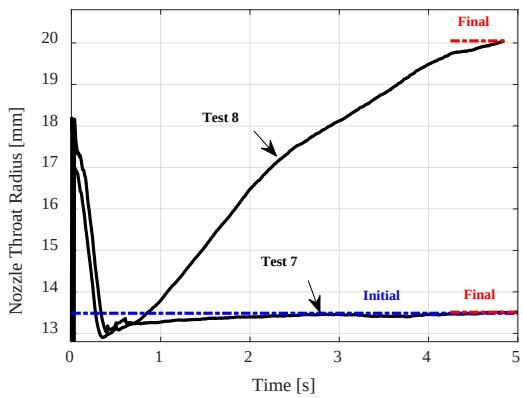

Figure 12. NTRT solutions for nozzle throat erosion history in Test 7 and Test 8. *SiC-coated graphite throat insert and CFRC throat insert;* A_r = 4.9 [-]

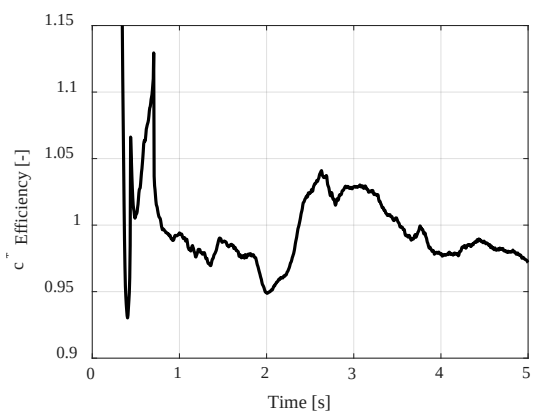

Figure 13. Method 2 solution for η^* history in Test 9.

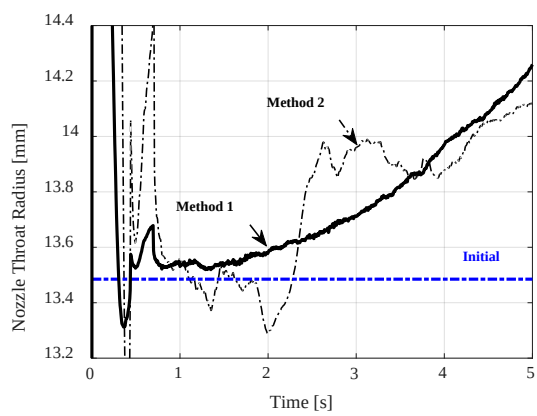

Figure 14. Comparison of solutions for nozzle throat erosion history in Test 9

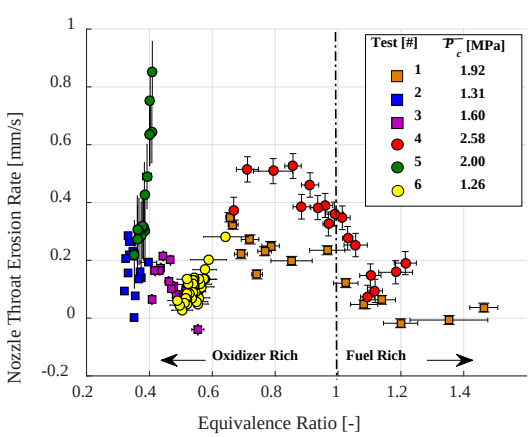

Figure 15. Equivalence ratio and nozzle throat erosion rate in Tests 1-6. *graphite nozzles; stoichiometric mixture ratio is* 3.429 [-]

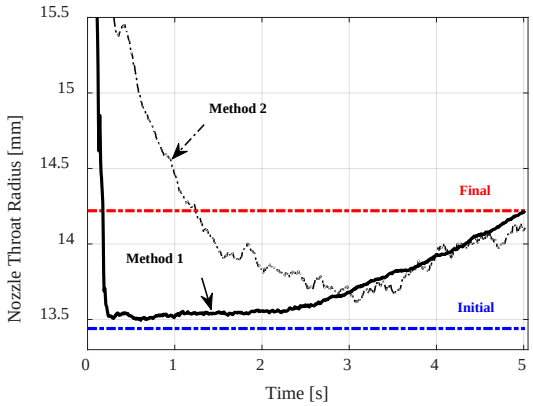

Figure 16. Comparison of solutions for nozzle throat erosion history in Test 1 determined by Method 1 (solid line) and Method 2 (dashed line).

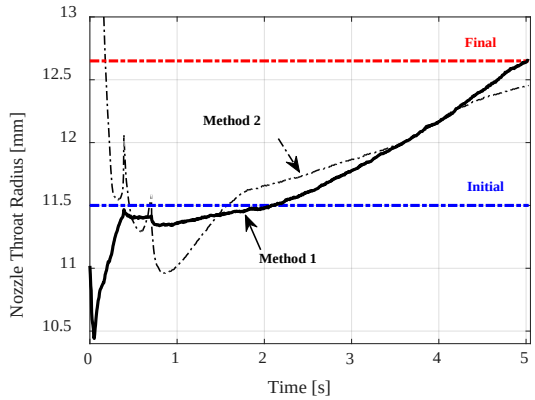

Figure 17. Comparison of solutions for nozzle throat erosion history in Test 4 determined by Method 1 (solid line) and Method 2 (dashed line).